Al-Nahrain Journal for Engineering Sciences **NJES** 26(4)343-350, 2023
http://doi.org/10.29194/NJES.26040343

Simulation of Effect a Variable Height of Porous Absorber on Ventilation Solar Chimney Performance

Suhaib J. Shbailat[1*], Mohammed A. Nima[2], Salwa Bouadila[3]

Authors affiliations:
1*) Mechanical Engineering Department, College of Engineering, Al-Nahrain University,
Baghdad, Iraq
suhaib.j.shbailat@nahrainuniv.edu.iq

2) Mechanical Engineering Department, College of Engineering, Baghdad University,
Baghdad, Iraq
mnima1@gmail.com

3) Research and Technology Center of Energy, Technopole of Borj Cedria Hammam Lif - B.P. 95, 2050, Tunisia
salwa.bouadila@crten.rnrt.tn

Paper History:

Received: 2nd Oct. 20xx

Revised: 9th Dec. 20xx

Accepted: 30th Jan. 2 0xx

Abstract

The improvement in solar chimneys' thermal performance and thermal behavior that can be achieved by adding metal foam has been tested in computational work. The flow and heat transfer governing equations for solar chimney models were solved using computational fluid dynamics (CFD). It was solved using the control volume numerical method in ANSYS FLUENT 14.5. It is used to construct a finite volume modeling technique for solving the governing equations and the radiation heat transfer equations. With standard flat absorber plates, the results showed that heat transmission was increased by the inclusion of metal foam (10 PPI), leading to an increase in air velocity at the solar chimney of around 13.3%. The highest average air velocity with 10 PPI drops by 54.4% as the height of the absorber plate changes from 5 cm to 25 cm respectively.

Keywords: Solar Chimney, Low Energy Space, Metal Foam, Simulation Modeling, Ventilation.

محاكاة تأثير الارتفاع المتغير للممتص المسامي على أداء المدخنة الشمسية للتهوية

صهيب جواد الشبيلات ، محمد عبد الرؤوف نعمة ، سلوى بوعديلة

الخلاصة:

تم اختبار التحسن في الأداء الحراري للمداخن الشمسية والسلوك الحراري الذي يمكن تحقيقه عن طريق إضافة الرغوة المعدنية في العمل الحسابي. تم حل المعادلات الحاكمة للتدفق وانتقال الحرارة لنماذج المداخن الشمسية باستخدام ديناميكيات الموائع الحسابية (CFD). تم حلها باستخدام طريقة التحكم العددية في حجم الصوت في ANSYS FLUENT 14.5. يتم استخدامه لبناء تقنية نمذجة الحجم المحدود لحل المعادلات الحاكمة ومعادلات انتقال الحرارة الإشعاعية. مع ألواح الامتصاص المسطحة القياسية، أظهرت النتائج أن انتقال الحرارة قد زاد عن طريق إدراج الرغوة المعدنية (١٠ PPI)، مما أدى إلى زيادة في سرعة الهواء في المدخنة الشمسية بحوالي ١٣,٣٪. أعلى متوسط لسرعة الهواء مع ١٠ نقطة في البوصة ينخفض بنسبة ٥٤,٤٪ مع تغير ارتفاع لوحة الامتصاص من ٥ سم إلى ٢٥ سم على التوالي.

1. Introduction

Solar power, one of several possible renewable energy sources, stands out for its low environmental impact and abundant local availability. Electricity generation, refrigeration, and air conditioning are just a few of the various uses for solar energy. Improve your building's natural ventilation with the help of solar energy by installing a solar chimney. Passive solar design refers to the practice of utilizing solar energy for thermal comfort without the use of any additional mechanical or electrical systems [1]. Aside from the windows, thermal mass, and chimney, other passive design components include this building's chimney. Passive solar energy cannot provide the necessary load effect on its own, especially for large buildings at night. For this reason, the vast majority of passive solar structures are hybrids, employing both passive and mechanical systems to obtain a low-energy result [2]. Air is supplied to and removed from a room through mechanical or natural processes to create ventilation.

A solar chimney, also known as an updraft stack, is a passive solar heating and ventilation system installed on the roof of a structure. When temperatures rise, proper air circulation and thermal comfort become paramount. Applications where low, steady temperatures are required favor solar chimneys. Buildings use natural means of conditioning air, while solar chimneys may help cut down on energy costs by minimizing the need for mechanical ventilation. This was found to be the case [3]. In order to better understand how the solar chimney with space ventilation can be used to enhance thermal

NJES is an **open access Journal** with **ISSN 2521-9154** and **eISSN 2521-9162**

performance and investigate the activity of an absorber media, a review of the work of past researchers is in order. Literature papers have shown a few different approaches to combining solar chimneys and space ventilation. To heat and ventilate the test building, [4] created a numerical analysis of heat transport in an SC system. The conservation equations were numerically solved using the finite difference method. There were fixed parameters in the governing equations. The Nusselt number Nu, the dimensionless volumetric flow rate v, and the radiation heat flux ratio q_r/q_{tot} were used as the controlling factors in these calculations. Consequently, isotherms and streamlines were generated.

[5] used a system consisting of an Evaporative Cooling Cavity (ECC) and a Solar Chimney (SC) to examine three different materials of cooling pad: coconut coir, vetiver, straw, and cellulose. It has been taken into account how the key geometric characteristics affect the system's efficiency. Human thermal comfort needs and the means to meet those needs have also been investigated. Results reveal that at a velocity of 0.10 m/s, the cellulose cooling pad achieves an efficiency of 47.5%, which is higher than the efficiency of a saturated heat exchanger. It demonstrated that increased wetted surface area and increased velocity lead to decreased contact time, leading to increased water evaporation into the air. [6] created a CFD model for a two-stage solar chimney using computational fluid dynamics. The steady-state transport equations for scalar and vector quantities (such as energy, turbulence, spectrum of radiation intensity, and vectors of velocity) are solved using a finite-volume technique. The fundamentals of 2D geometry were examined, and this was extended to cover three different solar chimney modifications for use in design and implementation. Based on the findings, it appears that the best performance was achieved by the solar chimney coupled with the single-opening type and ventilated rooms. [7] details the usage of a novel ecologically friendly solar chimney integrated with a windcatcher and water spray system to create a two-story office building suitable for a hot, dry region. Using the least amount of square footage possible, a solar chimney and windcatcher built on the north side of the building provide ventilation for both floors. To examine the cooling and ventilation possibilities of a solar chimney with and without a windcatcher, a reduced scale model and computational fluid dynamics (CFD) analysis were carried out. Researchers compare the results of testing conducted on days with much lower temperatures to show that the solar chimney, with a windcatcher and water spray system, provides appropriate thermal and airflow conditions for both floors on a hot and bright day. Cooling the occupied room by 5.2 degrees Celsius and producing around 9 air conditioning units per hour (ACH) during peak working hours is conceivable in the summer. [8] presented that solar chimneys can improve natural ventilation and cut down on solar heat gain on a building's exterior. In this study, we proposed three different ways to connect two solar chimneys to a heated wall for natural ventilation of a room: (I) in a series, (II) with the chimneys parallel and the air exhausting at two different points, and (III) with the chimneys parallel but the air exhausting at a single point. A Computational Fluid Dynamics model was used to forecast the airflow rate that would be attained with each setup. The data illustrate the impact of heat flux in each channel and channel geometry. In (II), the flow rate is maximized. To be more specific, the proposed configurations increase the flow rate by as much as 40% over the standard setup with a single-channel solar chimney. The research results suggest a new approach to façade design for mitigating the effects of solar heat gain and improving natural ventilation in buildings.

Previous research has shown that the passive solar chimney effect can be exploited for a variety of purposes, including heating, cooling, and ventilation. The buoyant force created is an effect shared by all modes.

The use of heat-absorbing material increases heat transfer and temperature differential, both of which have a multiplier effect on the buoyant force exerted by the air as it is evacuated by the solar chimney. While several computational studies have looked into using a flat plate as heat absorber media, few have considered whether or not the addition of porous materials to a solar chimney might improve its thermal performance. In this study, the effect of adding metal foam to a solar chimney to improve its thermal behavior is quantitatively explored.

2. Simulation modeling

The simulation model, which is based on governing equations (GE), depicts fluid flow, heat transmission, and heat storage in a variety of modes through a physical model and numerical simulation. Both a heating mode and a ventilation mode computational model are built. The use of both heating and cooling modes is ubiquitous in descriptions of physical models and numerical solutions. Both modes use ANSYS FLUENT version (14.5) to describe the steady-state heat transfer and fluid flow characteristics of air. In another section, we show how a mushy-zone material can temporarily store heat by combining the properties of a solid and a liquid.

2.1. Geometry

The solar chimney, test room, absorber flat plate, and Cooper foam absorber are all part of the SOLIDWORKS 2016 geometry models. The dimensions of the test chamber are (1m*1.5m*1.5m), and the dimensions of the solar chimney are (2m)(1m)(1m)(0.30m)(0.30m). Fiberglass was used to provide the 3cm thick thermal insulation. In Figure 1, we see the physical geometry of the system.

2.2. Governing Equations

Several assumptions have been established in order to generate a mathematical simulation for steady-state, free convection heat transfer in solar chimney ventilation.

i. Conservation equations in three dimensions.
ii. Incompressible-flow Steady-state.
iii. The density variation was modeled using the Boussinesq-approximation.
iv. A mean temperature is used to determine the value of each property.

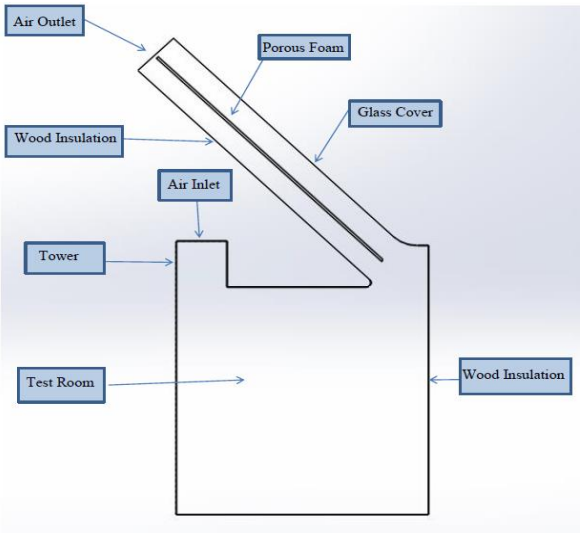

Figure (1): Model schematic including porous foam.

The conservation of mass, momentum, energy, and the equation of turbulence were crucial FLUENT modeling equations for fluid flow and heat transmission in the solar chimney via free convection. Cartesian notation allows for expressions like[9]:

Continuity Equation

$$\frac{\partial(\rho u)}{\partial x}+\frac{\partial(\rho v)}{\partial y}+\frac{\partial(\rho w)}{\partial z}=0 \qquad \text{…..(1)}$$

Momentum Equation

In x-direction is:

$$\frac{\partial(\rho uu)}{\partial x}+\frac{\partial(\rho uv)}{\partial y}+\frac{\partial(\rho uw)}{\partial z}$$
$$=-\frac{\partial p}{\partial x}+\frac{\partial}{\partial x}\left(\mu_{eff}\frac{\partial u}{\partial x}\right)+\frac{\partial}{\partial y}\left(\mu_{eff}\frac{\partial u}{\partial y}\right)$$
$$+\frac{\partial}{\partial z}\left(\mu_{eff}\frac{\partial u}{\partial z}\right)+S_u \qquad \text{……(2)}$$

In y-direction is:

$$\frac{\partial(\rho vu)}{\partial x}+\frac{\partial(\rho vv)}{\partial y}+\frac{\partial(\rho vw)}{\partial z}$$
$$=-\frac{\partial p}{\partial y}+\frac{\partial}{\partial x}\left(\mu_{eff}\frac{\partial v}{\partial x}\right)+\frac{\partial}{\partial y}\left(\mu_{eff}\frac{\partial v}{\partial y}\right)$$
$$+\frac{\partial}{\partial z}\left(\mu_{eff}\frac{\partial v}{\partial z}\right)+S_v \qquad \text{……(3)}$$

In z-direction is:

$$\frac{\partial(\rho wu)}{\partial x}+\frac{\partial(\rho wv)}{\partial y}+\frac{\partial(\rho ww)}{\partial z}$$
$$=-\frac{\partial p}{\partial z}+\frac{\partial}{\partial x}\left(\mu_{eff}\frac{\partial w}{\partial x}\right)+\frac{\partial}{\partial y}\left(\mu_{eff}\frac{\partial w}{\partial y}\right)$$
$$+\frac{\partial}{\partial z}\left(\mu_{eff}\frac{\partial w}{\partial z}\right)+S_w \qquad \text{……(4)}$$

Energy Equation

$$\frac{\partial(\rho uT)}{\partial x}+\frac{\partial(\rho vT)}{\partial y}+\frac{\partial(\rho wT)}{\partial z}$$
$$=\frac{\partial}{\partial x}\left(\Gamma_{eff}\frac{\partial T}{\partial x}\right)+\frac{\partial}{\partial y}\left(\Gamma\mu_{eff}\frac{\partial T}{\partial y}\right)+\frac{\partial}{\partial z}\left(\Gamma_{eff}\frac{\partial T}{\partial z}\right)$$
$$+S_T \qquad \text{……(5)}$$

Where the Reynolds stresses can be symbolized by equations (Awbi 2003):

$$S_{u=}\frac{\partial}{\partial x}\left(\mu_{eff}\frac{\partial u}{\partial x}\right)+\frac{\partial}{\partial y}\left(\mu_{eff}\frac{\partial v}{\partial x}\right)+\frac{\partial}{\partial z}\left(\mu_{eff}\frac{\partial w}{\partial x}\right)$$
$$+buoyancy \qquad \text{……(6)}$$

$$S_{v=}\frac{\partial}{\partial x}\left(\mu_{eff}\frac{\partial u}{\partial y}\right)+\frac{\partial}{\partial y}\left(\mu_{eff}\frac{\partial v}{\partial y}\right)+\frac{\partial}{\partial z}\left(\mu_{eff}\frac{\partial w}{\partial y}\right)$$
$$+buoyancy \qquad \text{……(7)}$$

$$S_{w=}\frac{\partial}{\partial x}\left(\mu_{eff}\frac{\partial u}{\partial z}\right)+\frac{\partial}{\partial y}\left(\mu_{eff}\frac{\partial v}{\partial z}\right)+\frac{\partial}{\partial z}\left(\mu_{eff}\frac{\partial w}{\partial z}\right)$$
$$+buoyancy \qquad \text{……(8)}$$

And the heat source;

$S_{T=}\ 0$

buoyancy(for u) = $\rho g\beta\ (T_f - T_{in})\cos(\theta)$

buoyancy(for v) = $\rho g\beta\ (T_f - T_{in})\sin(\theta)$

θ : Incline angle of the chimney

$\Gamma_{eff}=\frac{\mu_{eff}}{\delta_{eff}}+\frac{\mu_t}{\delta_t}$

$\mu_{eff}=\mu+\mu_t$

μ_{eff} = coefficient of effective viscosity

Γ_{eff} = coefficient of effective diffusion

δ_{eff} = effective Prandtl number

Turbulence Model

The Standard k-e Model

The most popular model in Fluent is the standard k-epsilon (k-) model because of its accuracy, low computational cost, and general applicability to completely turbulent flows. The following equation [10] be used to calculate the turbulent kinetic energy and dissipation rate; this model is an example of a two-equation model.

Turbulent Kinetic Energy

$$\frac{\partial}{\partial x}(\rho uK`)+\frac{\partial}{\partial y}(\rho vK`)+\frac{\partial}{\partial z}(\rho wK`)$$
$$=\frac{\partial}{\partial x}\left[\Gamma_k\frac{\partial K`}{\partial x}\right]+\frac{\partial}{\partial y}\left[\Gamma_k\frac{\partial K`}{\partial y}\right]+\frac{\partial}{\partial z}\left[\Gamma_k\frac{\partial K`}{\partial z}\right]+P_k+G_k$$
$$-C_D\rho\varepsilon \qquad \text{……(9)}$$

Where;

$\Gamma_k=\frac{\mu_{eff}}{\sigma_K}$

σ_K = empirical constant of turbulent Prandtl number for kinetic energy

Dissipation Rate

$$\frac{\partial}{\partial x}(\rho u\varepsilon)+\frac{\partial}{\partial y}(\rho v\varepsilon)+\frac{\partial}{\partial z}(\rho w\varepsilon)$$
$$=\frac{\partial}{\partial x}\left[\Gamma_\varepsilon\frac{\partial \varepsilon}{\partial x}\right]+\frac{\partial}{\partial y}\left[\Gamma_\varepsilon\frac{\partial \varepsilon}{\partial y}\right]+\frac{\partial}{\partial z}\left[\Gamma_\varepsilon\frac{\partial \varepsilon}{\partial z}\right]+C_{\varepsilon1}\frac{\varepsilon}{k}(P_k$$
$$+C_{\varepsilon3}G_k)-C_{\varepsilon2}\rho\frac{\varepsilon^2}{k} \qquad \text{……(10)}$$

Where;

$\Gamma_\varepsilon=\frac{\mu_{eff}}{\sigma_\varepsilon}$

σ_ε = empirical constant of turbulent Prandtl number for ε

The production of k by shear, this term can be expressed as following [11]:

$$P_k=\mu_t\left[2\left(\frac{\partial u}{\partial x}\right)^2+2\left(\frac{\partial v}{\partial y}\right)^2+2\left(\frac{\partial w}{\partial z}\right)^2\right.$$
$$+\left(\frac{\partial u}{\partial y}+\frac{\partial v}{\partial x}\right)^2+\left(\frac{\partial w}{\partial y}+\frac{\partial v}{\partial z}\right)^2$$
$$\left.+\left(\frac{\partial w}{\partial x}+\frac{\partial u}{\partial z}\right)^2\right] \qquad \text{……(11)}$$

The turbulence kinetic energy generation by buoyancy represented in term G_k, this term can be expressed as following [11]:

$$G_k = \frac{\mu_t}{\sigma_t} g\beta \frac{\partial T}{\partial y} \quad \ldots\ldots (12)$$

where the turbulent viscosity μ_t is given by:

$$\mu_t = \rho C_\mu \frac{k^2}{\varepsilon} \quad \ldots\ldots (13)$$

2.2.1. Mathmatical Model Porous Media

Using copper foam as an absorbing media in the solar chimney is innovative in the current work. Since the thickness of porous metal foam is negligible in comparison to the length of porous metal foam [12] porous jump is an appropriate approach that can be used to build this model. The physics of airflow via the pore structure can be explained and accounted by mathematical models [13]:

Continuity Equation:

$$\nabla . \left(\rho \vec{V} \right) = 0 \quad \ldots\ldots (14)$$

Momentum Equation:

$$\frac{\rho}{\phi} \langle (\vec{V} \nabla) \vec{V} \rangle = -\nabla \rho + \mu_{eff} \nabla^2 \langle \vec{V} \rangle - \left[\frac{\mu_f}{K} + \frac{\rho F}{\sqrt{K}} |\vec{V}| \right] \langle \vec{V} \rangle + \rho g \beta \, (T_f - T_{in}) \quad \ldots\ldots..(15)$$

Energy equation in the fluid region

$$\rho_f \left[\langle \vec{V} \rangle . \nabla T_f \right] = \nabla . \left[\left(\frac{\mu}{Pr} + \frac{\mu_t}{Pr_t} \right) \nabla T_f + h_{sf} \, a_{sf} / Cp \, (T_s - T_f) \right] \quad \ldots (16)$$

Energy equation in the solid region

$$(\rho \, cp)_s \left(\frac{\partial T_s}{\partial t} \right) = 0 = \nabla . [k_s \nabla T_s] - h_{sf} \, a_{sf} \, (T_s - T_f) \quad \ldots\ldots (17)$$

(k_s) solid matrix thermal conductivity $(W/m.k)$
(ϕ) porosity of the porous medium
(h_{sf}) interfacial heat transfer coefficient $(w/m^2.k)$
(a_{sf}) solid-liquid interfacial surface area of porous layer (m)
(cp_s) specific heat of solid matrix $(J/kg.k)$

Where k is the permeability, μ_f is the dynamic viscosity of the fluid, and F is defined by Kozeny-Carman of the inertia coefficient of the porous media and the correction equation can be written as follows [14]. Table 4 presents the measured permeability coefficient, inertial coefficient, and porosity of metal foam.

$$k = \frac{d_p^2 \, \phi^2}{175 \, (1 - \phi)^2} \quad \ldots\ldots (18)$$

$$F = \frac{1.75}{\sqrt{175} \; \phi^{3/2}} \quad \ldots\ldots (19)$$

2.2.2. The Discrete Ordinate (DO) Model

Radiation heat transfer using the discrete ordinates model. Semitransparent surfaces and large variations in optical thickness are the exclusive domain of this mode.

For an absorbing, scattering material emitting in the direction s at location r, the radiative transfer equation (RTE) is [15]:

$$\nabla . (I(\vec{r}, \vec{s}) \vec{s}) + (a + \sigma_s) \, I(\vec{r}, \vec{s}) = a \, n^2 \frac{\sigma T^4}{\pi} + \frac{\sigma_s}{4\pi} \int_0^{4\pi} I(\vec{r}, \vec{s}') \, \varphi(\vec{r}, \vec{s}') \, d\Omega \quad \ldots\ldots (20)$$

Where;
$I(r,s)$ is the solar radiation intensity,
(a) is the coefficient of the absorption,
(n) is the refractive index,
(σ) is Stefan - Boltman constant,
(σs) is the coefficient of the scattering.

3. Computational modeling

3.1. CFD Model Setting and Parameter

Momentum and energy equations were solved using an upwind approach of second order, while pressure was solved using a simple standard method. Pressure was relaxed by a factor of 0.3, density by a factor of 1, body forces by a factor of 1, momentum by a factor of 0.7, and energy by a factor of 1. Models (I) and (II), as shown in Figure 2, required (1200) to (1400) iterations until the flow solution converged, at which point the residuals in the energy and continuity equations were respectively 800 and 1000. After (1200–125) iterations in this model, the flow solution was found to converge when the residuals in the energy and continuity equations were respectively 700 and 300.

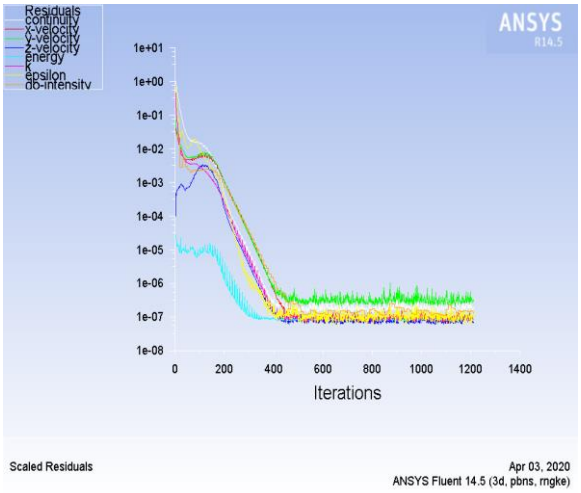

Figure (2): ANSYS-FLUENT Iterations of the Case

3.2. Meshing

For a simulation in ANSYS FLUENT to successfully converge on a solution that accounts for all relevant parameters, the mesh must be of sufficient quality. Boundary layer flow and temperature gradients can only be accurately represented in the current simulation if enough nodes are located in the vicinity of the boundaries. With too many nodes, processing takes longer and uses more resources without improving resolution. Both fluid dynamics and heat transport require a mesh fine enough to capture the relevant information [16]. Figure 3 displays the mesh produced for this work, which was determined to be sufficiently fine to capture the relevant features of fluid

movement and heat transmission from numerous experimental runs.

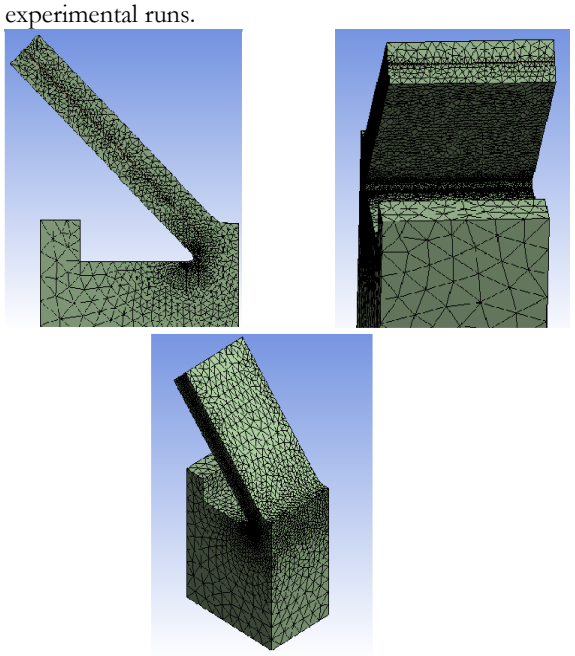

Figure (3): 3-D Mesh grid of models with metal foam.

3.3. Boundary Conditions

Table1 displays the associated boundary conditions required to finalize the formulation of the present work.

Table (1): Boundary condition of the physical-model

Boundary	Type	Parameter value
Tower inlet	Pressure inlet	Ambient Temperature Atmospheric Pressure
Chimney outlet	Pressure outlet	Ambient Temperature Atmospheric Pressure
Absorber plate	Wall	Mixed Convection and Radiation
Glass roof	Wall	Mixed Convection and Radiation
Room	Wall	Fixed Heat Flux

3.4. Material Properties in Fluent

Table 2 and Figure 4 summarize the relevant material features.

Table (2): Physical properties of materials [17].

Physical property	Absorber plate	Glass roof	Insu-lation	Air
Density kg/m³	8978	1900	700	Boussi-nesq
Specific heat J/kg.K	381	837	2310	1006.43
Thermal Conductivity W/m.K	387.6	0.91	0.137	0.0242
Viscosity kg/m.s	-	-	-	1.789e-5
Refractive index	1	1.562	1	1

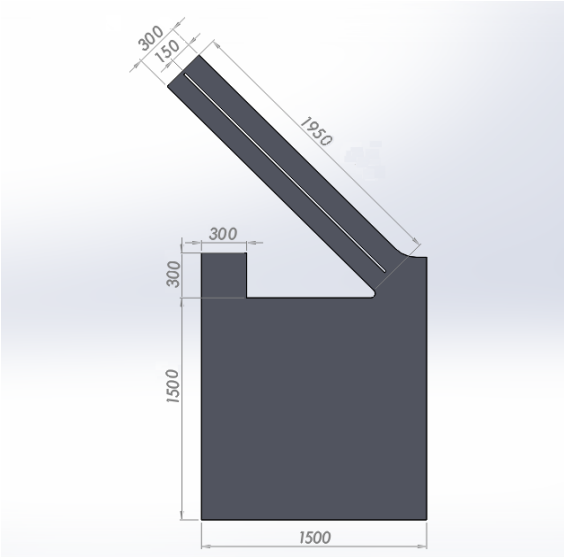

Figure (4): Schematic-diagram of physical domain(mm).

3.5. Operating Conditions

The present work uses an operating pressure of 101.325 Kpa, a reference pressure location of (0, 0), and gravity components of (x= 0 m/s², y= -9.81 m/s², z=0 m/s²) for both inclined and vertical channels. The porous metal foam's features and circumstances are listed in Table 3.

Table (3): Properties condition of the metal-foam[18].

Pores per inch (PPI)	Porosity (p) (%)	Permeability (K)(m²)	Inertial Coefficient (C)
10	0.93	7.859×10^{-8}	0.17

In this paper, the density of air was calculated using the Boussinesq model [19],

$$\varrho = \varrho o\,[1 - \beta\,(T - To)] \qquad \ldots\ldots (21)$$

When the input temperature is set the density at T_o is o, the density at T is a, and the thermal expansion coefficient is β.

3.6. Grid Independence Test

The appropriate mesh was determined by an examination of grid independence. The speed via the chimney was the object of the experiment. A total of seven distinct grids were examined, each with 187,353 elements: 1,162,122, 591,543, 842,651, 966,531, and 1,296,425 elements. For the most exacting measurements of the chimney's velocity, there are minor discrepancies (usually less than 5 percent) between the data from grid no. 6 (1,162,122 elements) and grid no. 7 (1,296,425 elements). It can be seen in figure 5 that both grids are getting closer to being grid independent [20].

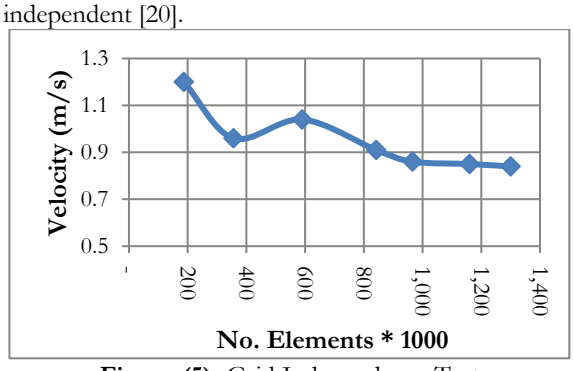

Figure (5): Grid Independency Test

4. Simulation results

4.1. Temperature Distribution

Figures (5-10) depict the temperature contour behavior for a 10 PPI metal foam absorber plate at various solar radiation intensities (953 W/m²), inclination angles (45⁰), and absorber plate heights (5, 10, 15, 20, 25 cm). The temperature profile and metal foam absorber plate both rise with increasing plate height, with H=25cm representing their maximum value. Because the boundary layer spread over the metal foam as the absorber plate height was increased, conduction heat became more predominant than convective heat, and the temperature of the absorber plate rose because of the lack of heat exchange between the air and the metal foam.

The results demonstrate that the room temperature is very near to the ambient temperature after the highest value of solar irradiation because the solar chimney suctions the air from the outside into the test room, which is presumably well insulated. This creates a hostile environment for people, but it can be converted into a soothing breeze with some tweaking. Alternately, the ventilation effect can be utilized at varying times of the day and night to eliminate noxious gases and aromas from rooms, auditoriums, and workshops.

4.2. Air Pathlines

Air pathlines for metal foam absorber plate (10 PPI) at the same solar radiation intensity (I= 953 W/m²) and for inclination angle 45° are shown in Figures (11-16). The heights of the absorber plates varied from 5 cm, 10 cm, 15 cm, 20 cm, and 25 cm.

The average air velocity of the solar chimney is found to grow as the absorber plate height drops, with the optimal value being attained when the absorber plate height is only 5 cm. Due to the expansion of the boundary layer above the metal foam as the absorber plate height was increased, the potential energy and buoyancy force could not be employed to increase the flow through the metal foam, and so no heat exchange occurred. Therefore, the air velocity of the solar chimney was decreased due to the airflow of the top and lower absorber plate at H= 20 cm and H= 25 cm.

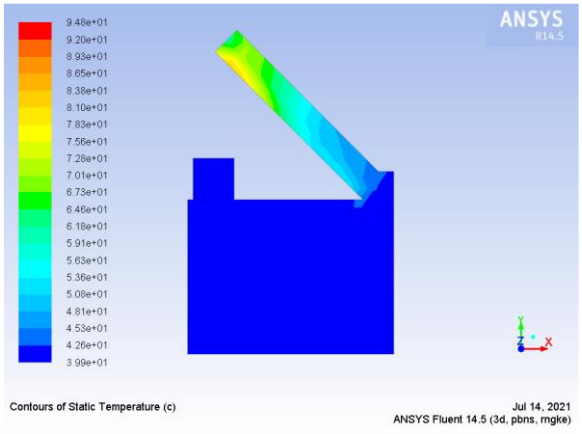

Figure (6): Temp. Contour of Flat Absorber Plate

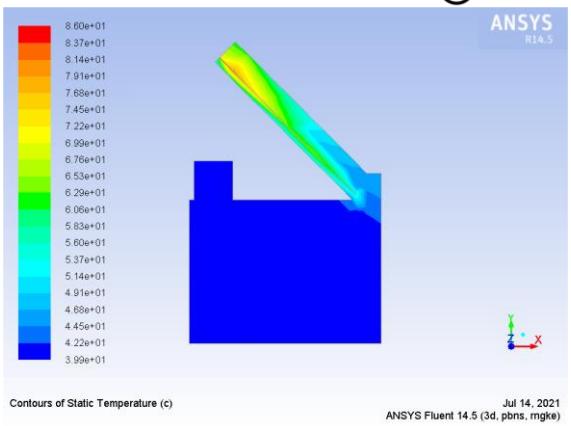

Figure (7): Temp. Contour of 10 PPI Metal Foam H= 5 cm

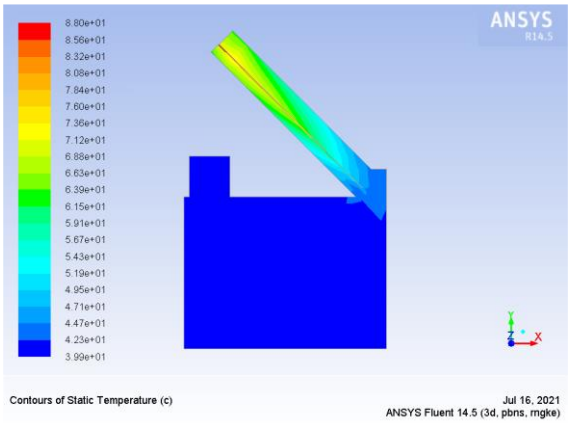

Figure (8): Temp. Contour of 10 PPI Metal Foam H= 10 cm

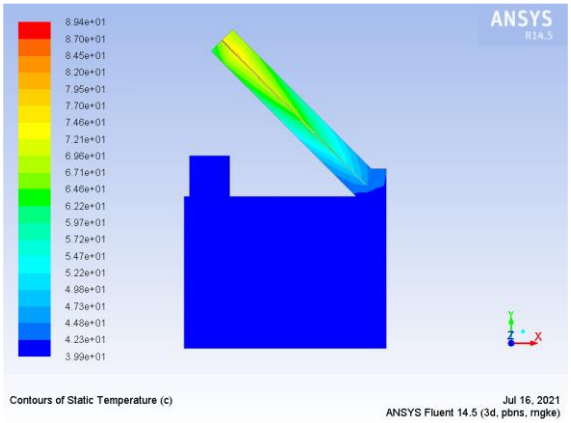

Figure (9): Temp. Contour of 10 PPI Metal Foam H= 15 cm

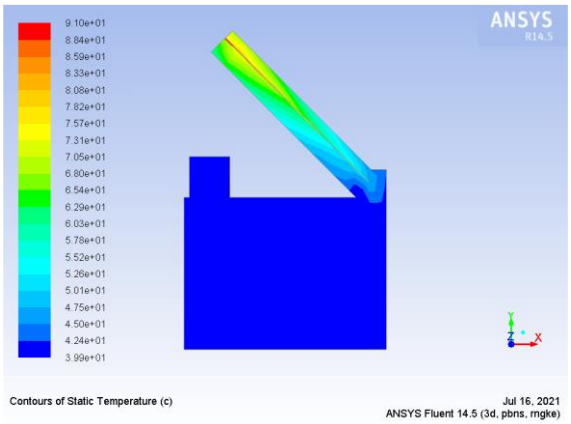

Figure (10): Temp. Contour of 10 PPI Metal Foam H=20 cm

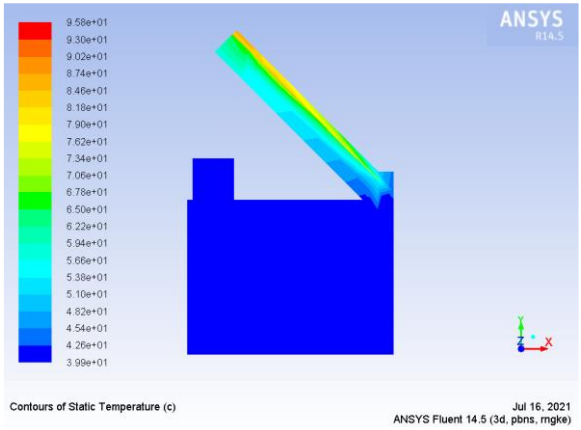

Figure (11): Temp. Contour of 10 PPI Metal Foam H=25 cm

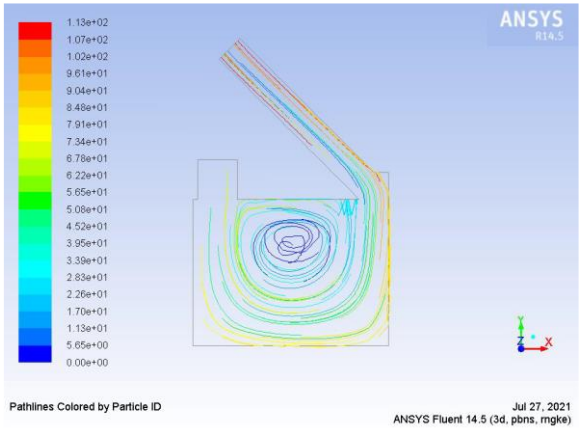

Figure (12): Velocity Pathline of Flat Absorber Plate

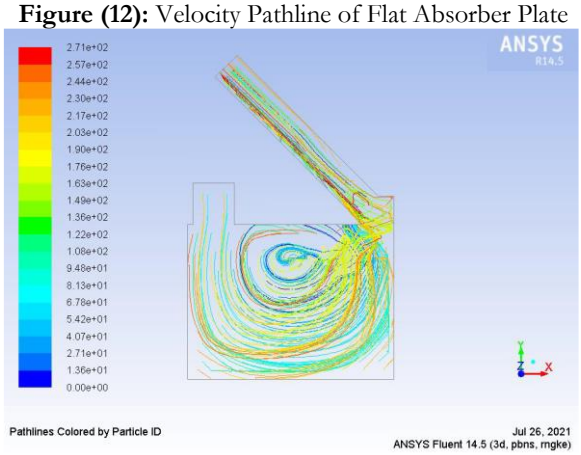

Figure (13): Velocity Pathline of 10 PPI Metal Foam H= 5 cm

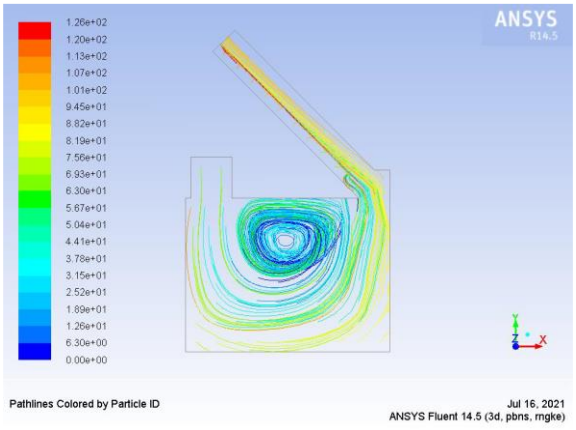

Figure (14): Velocity Pathline of 10 PPI Metal Foam H= 10cm

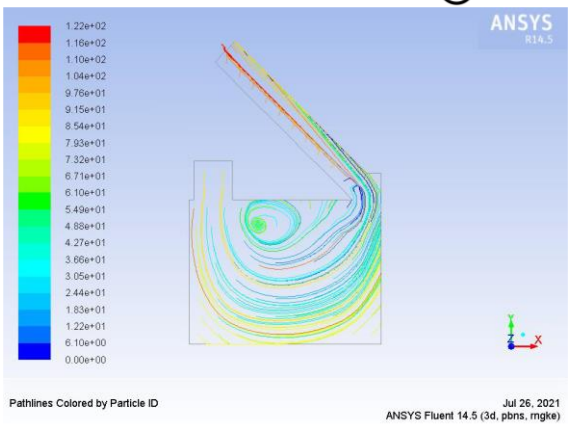

Figure (15): Velocity Pathline of 10 PPI Metal Foam H= 15cm

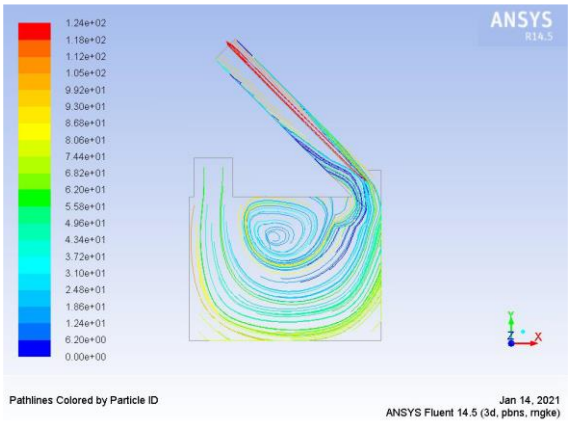

Figure (16): Velocity Pathline of 10 PPI Metal Foam H= 20cm

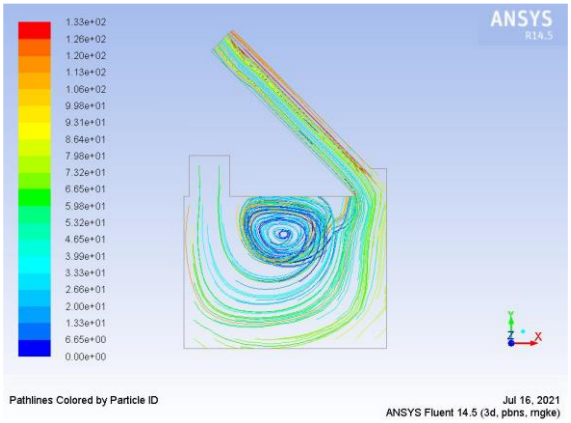

Figure (17): Velocity Pathline of 10 PPI Metal Foam H= 25cm

5. Conclusion

The integration of the test room and solar air chimney with (10) PPI metal foam absorber plates in the solar air chimney and with five different heights of absorber plate from 5 cm, 10 cm, 15 cm, 20 cm, and 25 cm has been studied numerically to determine the effect on heat transfer characteristics and overall performance.

The current work led to the following conclusions, the heat transmission was increased by the inclusion of metal foam (10 PPI), leading to an increase in air velocity at the solar chimney of around 13.3%. The highest average air velocity with 10 PPI drops by 54.4% as the height of the absorber plate changes from 5 cm to 25 cm respectively.

6. References

[1] Shbailat, Suhaib J.; Nima, Mohammed A. Possible energy saving of evaporative passive cooling using a solar chimney of metal foam porous absorber. Energy Conversion and Management: X, 2021, 12: 100118.

[2] Clive, Beggs. Energy: management, supply and conservation. Routledge, (2010).

[3] Nadia, Saifi, Noureddine Settou, Boubekeur Dokkar, Belkhir Negrou, and Nasreddine Chennouf. "Experimental study and simulation of airflow in solar chimneys." Energy Procedia 2012 18: 1289-1298.

[4] Nouanégué, H. F., and E. Bilgen. "Heat transfer by convection, conduction and radiation in solar chimney systems for ventilation of dwellings." International Journal of Heat and Fluid Flow 30, 2009 no. 1: 150-157.

[5] Kumar, Madhan Anand, and U. Krishnaveni. "Analysis of solar chimney with evaporative cooling cavity to improve indoor air quality." Journal of Chemical and Pharmaceutical Sciences 2015 ISSN 974: 2115.

[6] Baxevanou, Catherine, and Dimitris Fidaros. "Numerical Study of Solar Chimney Operation in a two story Building." Procedia Environmental Sciences 2017 38: 68-76.

[7] Kazemi Iman, Moosavi, Leila, Majid Zandi, Mokhtar Bidi, and Ehsan Behroozizade. "New design for solar chimney with integrated windcatcher for space cooling and ventilation." Building and Environment 2020 181: 106785.

[8] Nguyen, Y. Quoc, Viet T. Nguyen, Long T. Tran, and John C. Wells. "CFD Analysis of Different Ventilation Strategies for a Room with a Heated Wall." Buildings 12, no. 9 2022: 1300.

[9] Ali Ghaffari and Ramin Mehdipour. Modeling and Improving the Performance of Cabinet Solar Dryer Using Computational Fluid Dynamics. Int. J. Food Eng. 2015; 11(2): 157–172

[10] Calmidi V. V., and Mahajan R. L. Forced convection in high porosity metal foams. Journal of Heat Transfer, 2000; 122 (8): 557.

[11] Guo C.X., Zhang W.J., and Wang D.B. Numerical investigation of heat transfer enhancement in latent heat storage exchanger with paraffin/graphite foam. 10th Int. Conf. on Heat Transfer, Fluid Mechanics and Thermodynamics 2014; July: 14 – 26.

[12] Ali, S.A.G. Study the effect of upstream riblet on wing- wall junction. M.Sc, Thesis, University of Technology, Iraq. 2011.

[13] Abdul Hussein SA, Shbailat SJ. Impact of bumpers position variation on heat exchanger performance: an experimental and predictive analysis using an artificial neural network. Journal of Engineering and Applied Science. 2023 Dec;70(1):1-20.

[14] Shbailat SJ, Rasheed RM, Sherza JS, Ansam AM. Effect of inserting 10-PPI copper foam as a porous absorber on the solar cooker performance. International Journal of Advanced Technology and Engineering Exploration. 2023 Sep 1;10(106):1225.

[15] Shbailat SJ, Rasheed RM, Muhi RJ, Mohammed AA. Effect of the 40-PPI copper foam layer height on the solar cooker performance. Open Engineering. 2023 Sep 30;13(1):20220471.

[16] Shbailat SJ, Nima MA. Effect of absorber plate height on the performance of solar chimney utilized with porous absorber and integrated with an insulated room. Thermal Science. 2022;26(6 Part A):4775-95.

[17] Hussein SA, Shbailat SJ. Experimental and numerical study of forced convictive heat transfer in a horizontal circular pipe with varying angles ribs. International Journal of Advanced Technology and Engineering Exploration. 2022 Aug 1;9(93):1246.

[18] Mohammed AA, Mohammed AA, Channapattanac SV. Experimental Investigation into Natural Convection Heat Transfer inside Triangular Enclosure with Internal Hot Cylinder. Al-Nahrain Journal for Engineering Sciences , 2023 Oct.31;26(3):175-8.

[19] Mohammed AA, Salman AM. Characteristics of Flow-Induced Vibration of Conveying Pipes for Water and Coolant Flow. Journal of Advanced Research in Fluid Mechanics and Thermal Sciences. 2023 Jul 25;106(2):177-93.

[20] Bouadila S, Rehman TU, Baig MA, Skouri S, Baddadi S. Energy, Exergy and Economic (3E) analysis of evacuated tube heat pipe solar collector to promote storage energy under North African climate. Sustainable Energy Technologies and Assessments. 2023 Feb 1;55:102959.

Appendix I: Nomenclature

Symbol	Definition	Units
α_f	Thermal Diffusivity	m^2/s
β	Volumetric Thermal Expansion	1/K
ε	Porosity, Emissivity	-
η	Thermal efficiency	%
θ	Incidence Angle	Degree
μ	Dynamic Viscosity	kg m/s
ν	Kinetic Viscosity	m^2/s
ρ	Density	kg/m^3
σ	Stefan – Boltzmann Constant	$W/m^2.K^4$
α_f	Thermal Diffusivity of Fluid	m^2/s
α	Absorptivity Coefficient	-
Do	Radiation Desecrate Ordinate	
CFD	Computational Fluid Dynamic	
Conv	Convection	
MF	Metal Foam	
PPI	Pore Per Inch	
Rad.	Radiation	
RNG	Re-Normalization Group	
SC	Solar Chimney	